HIROSAKI UNIVERSITY

Radiation Environment and Medicine 2019 Vol.8, No.1 9–15

REM
Radiat Environ Med

Regular Article

Quantitative and Visual Image Quality Evaluation between CsI and Gd_2O_2S:Tb Scintillator Types of Irradiation Side Sampling Flat-Panel Detector Systems for Reduction of Radiation Exposure

Kohsei Kudo[1]*, Minoru Osanai[1], Megumi Tsushima[1], Junichi Hirota[1], Yuhiko Otani[2], Satoshi Naraki[2], Katsumasa Suzaki[2], Masahiko Aoki[2, 3] and Yoichiro Hosokawa[1]

[1]*Department of Radiation Science, Hirosaki University Graduate School of Health Sciences, 66-1 Hon-cho, Hirosaki, Aomori 036-8564, Japan*
[2]*Department of Radiology, Hirosaki University School of Medicine and Hospital, 53 Hon-cho, Hirosaki, Aomori 036-8563, Japan*
[3]*Department of Radiology and Radiation Oncology, Hirosaki University Graduate School of Medicine, 5 Zaifu-cho, Hirosaki, Aomori 036-8562, Japan*

Received 20 March 2018; revised 4 July 2018; accepted 8 August 2018

Flat-panel detector (FPD) systems have been widely used instead of computed radiography (CR) systems for radiation diagnosis. Indirect FPD systems have either CsI or Gd_2O_2S:Tb (GOS) types of scintillators. CsI FPDs can achieve comparable image quality whilst using lower dose imaging than GOS FPDs. Additionally, irradiation side sampling FPDs (ISS-FPDs) have better resolution characteristics than penetration side sampling FPDs (PSS-FPDs). In order to investigate exposure dose reduction, an analysis of both quantitative image quality metrics and visual evaluation of CsI and GOS ISS-FPDs was performed. Image quality was evaluated by detective quantum efficiencies and contrast-to-noise ratios, whilst visual evaluation was performed by inverse image quality figures (IQFinv) and area under the curves (AUCs) of the receiver operating characteristic (ROC) curves. The results suggest that CsI can produce comparable images to GOS with a dose reduction of 42-44% according to the image quality evaluation and 37-46% according to the visual evaluation.

Key words: flat-panel detector, CsI, Gd_2O_2S:Tb, reduction of radiation exposure, image quality

1. Introduction

Flat-panel detector (FPD) systems have been used for clinical imaging diagnosis since 1998[1, 2]. FPDs with direct conversion or indirect conversion systems[2] are now commonly used in clinical practice[3]. The scintillators using indirect FPDs are either of the CsI or the Gd_2O_2S:Tb (GOS) types[4]. Both CsI and GOS FPDs have a high resolution irradiation side sampling flat-panel detector (ISS-FPD) that detects fluorescence in the front compared to conventional penetration side sampling flat-panel detectors (PSS-FPDs)[5, 6].

Patient exposure in radiation diagnosis is classified as medical exposure and also as planned exposure[7]. For medical exposure, dose limits are not applicable as they should not hinder the effect of the required radiological diagnostic ability. For planned exposure, diagnostic reference levels (DRLs) are used for patient protection in radiation diagnosis[7, 8]. In Japan, DRLs were published in 2015[9]. These guidelines state that DRLs are a tool for identifying facilities with unusually high

*Kohsei Kudo : Hirosaki University Graduate School of Health Sciences, 66-1 Hon-cho, Hirosaki, Aomori 036-8564, Japan
E-mail: kohsei@hirosaki-u.ac.jp

Copyright © 2019 by Hirosaki University. All rights reserved.

Table 1. Details of the irradiation side sampling flat-panel detectors (ISS-FPDs) used in this study

Type of ISS-FPD system	CsI	GOS*
Manufacturer	FUJIFILM Corporation	FUJIFILM Corporation
Product name	MobileDaRt Evolution	CALNEO C1717 Wireless
System name	DR-ID 800	DR-ID 600
Detector, Panel unit	Scintillator (CsI), DR-ID 611SE	Scintillator (Gd_2O_2S:Tb), DR-ID 602SE
Grid	No grid	No grid
Console	DR-ID800CL	DR-ID300CL
Pixel size (mm)	0.15	0.15
Bit depth (bits)	10	12

*GOS: Gd_2O_2S: Tb

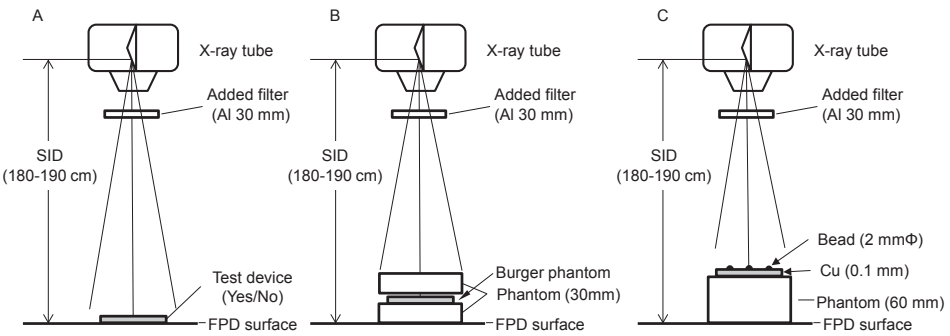

Fig. 1. Geometrical arrangements for the experiments. A: for digital characteristic curve, pre-sampled modulation transfer function (MTF), normalized noise power spectrum (NNPS), and detective quantum efficiency (DQE). B: for contrast-to-noise ratio (CNR) and inverse image quality figure (IQFinv). C: for the area under the curve (AUC) of the receiver operating characteristics (ROC) curve. SID = source-image receptor distance; FPD = flat-panel detector.

doses and for promoting the dose optimization process, and that in general the equipment performance and protocols (procedures) are investigated. Therefore, dose optimizations should be made while maintaining image quality.

There are reports that GOS ISS-FPD systems can reduce exposure dose by approximately 50% when compared to conventional computed radiography (CR)[10, 11]. It has also been reported that CsI FPD systems have a better detective quantum efficiency (DQE) than GOS FPD systems[3, 12]. However, ISS and PSS were not mentioned in these studies, and there has been no report comparing CsI and GOS ISS-FPD systems. Therefore, in this study we investigated image quality and visual evaluation of CsI and GOS type ISS-FPD systems for the purpose of reducing exposure dose.

2. Materials and Methods

For image quality evaluation, pre-sampled modulation transfer functions (MTFs), normalized noise power spectrums (NNPSs), and DQEs were measured in conformity with the International Electrotechnical Commission (IEC) 62220-1[13] at radiation qualities of RQA7[14]. RQA7 was selected based on the clinical use situation. Contrast-to-noise ratios (CNRs)[15, 16] were also measured. For visual evaluation, the inverse image quality figure (IQFinv)[17, 18] of a Burger phantom, and area under the curves (AUCs) of the receiver operating characteristic (ROC) curve were calculated[19, 20].

2.1. Equipment, radiation quality, incident dose and image analysis

A CsI type (MobileDaRt Evolution, FUJIFILM Corporation, Tokyo, Japan) and a GOS type ISS-FPD system (CALNEO C1717 Wireless, FUJIFILM Corporation) were used. The details of the digital imaging systems are shown in Table 1. For the CsI type ISS-FPD system, a MobileDaRt digital mobile X-ray system (MobileDaRt Evolution, Shimadzu, Kyoto, Japan) equipped with a portable FPD was used. For the GOS type ISS-FPD system, an X-ray generator (UD150B-40, Shimadzu) and an X-ray tube (P364DK-85, Shimadzu) were used. Experiments were conducted at a source-image receptor distance (SID) within the range of 180-190 cm.

Experimental arrangement conformed to IEC62220-1[13] (Fig. 1). For evaluating the radiation quality of X-ray beams, an RQA7 [additional filtration 30.0 mm A1, half-value layer (HVL) 9.1 mm A1] was used[13, 14]. The reference incident dose was set to 8.76 μGy (1 mR), and irradiation was performed within the range of $1/50^{th}$ to 32 times the reference dose, according to the needs for

measuring digital characteristic curves, MTFs, NNPSs, CNRs, IQFs, and AUCs. For measurements of incident doses and HVLs, a semiconductor detector (RaySafe Xi, Uniforce RaySafe, Billdal, Sweden) was used. For comparison between systems, all of the pixel values were converted and linearized from the original Digital Imaging and Communications in Medicine (DICOM) images to relative exposure images in ImageJ [National Institutes of Health (NIH), Bethesda, USA.

2.2. Image quality evaluation

2.2.1. Digital characteristic curve, pre-sampled MTF, NNPS, and DQE

Digital characteristic curves, pre-sampled MTFs, NNPSs, and DQEs of the CsI and the GOS were measured and compared. The geometric arrangements are shown in Figure 1A. For specific details of the measurements, we referred to "Image quality measurement of digital radiography, Ohm-sha, Tokyo, Japan,"[21] conforming to IEC 62220-1. Acquisition of digital image data was carried out with a fixed sensitivity ("S" value) of 200 and a latitude ("L" value) of 4[11, 22] in the test mode for both CsI and GOS.

The digital characteristic curves were used for linearization. Therefore, the doses for preparation of digital characteristic curves do not cover the dynamic range. Pre-sampled MTFs were derived from the average value of three independent measurements. NNPSs were selected from images evenly irradiated under various exposure conditions. With measured average pre-sampled MTFs and an NNPS at the reference dose used, the DQEs in both the vertical and the horizontal directions were calculated by:

$$\mathrm{DQE}\ (u) = \frac{\text{presampled MTF}^2\ (u)}{\mathrm{NNPS}\ (u) \cdot q}$$

where u is the spatial frequency (cycles/mm), and q is the number of incident photons. The number of photons was 32362 [1/(mm^2 ·μGy)] at RQA7[14]. Nyquist frequencies for both the CsI and GOS were 3.3 cycles/mm.

2.2.2. Contrast-to-Noise Ratio

As shown in Figure 1B, a convex Burger phantom was used. In order to add scatter, the Burger phantom was sandwiched between Mix-Dp (30 mm) phantoms. The average relative exposure of the pixel value and standard deviation of a circular region of interest with a diameter of 50 pixels at the convex part (diameter 10 mm, height 5 mm) are m_1 and σ_1, and those of the flat part are m_2 and σ_2. CNRs were calculated by[15, 16]:

$$\mathrm{CNR} = \frac{|m_1 - m_2|}{\sqrt{\frac{\sigma_1^2 + \sigma_2^2}{2}}}$$

2.3. Visual evaluation

2.3.1. IQFinv

For IQFinv, the convex Burger phantom was placed at the position shown in Figure 1B. Seven observers, using a 5-mega-pixel high-definition monitor, calculated IQFinv as[17-19]:

$$\mathrm{IQFinv} = \frac{100}{\sum_{i=1}^{n} (Di * hi)}$$

where Di is the size (mm) of the diameter of each Burger phantom, and hi is the identifiable minimum height (mm). Higher IQFinv values indicate visually superior quality.

2.3.2. Area Under the Curve

For the ROC analysis, acrylic beads (2 mm diameter) were placed on a copper plate (0.1 mm thickness) as shown in Figure 1C. The copperplate was divided into 30 sections, and acrylic beads were placed in 15 arbitrary sections, with 15 sections producing no signal and 15 sections producing signal for each capture. The position of the acrylic beads was changed under each irradiation condition and captured three times, with a total of 90 data captures per condition. Five observers assessed image quality using a 5-level rating. The ROC curve was computed by averaging the individual observations and the AUC of the ROC curve was calculated[19, 20]. The software used for the calculations was WROCFIT, created by Ogawa W[20].

There were no special reasons for visual evaluation using IQFinv and ROC, although the number of observers for each differed (7 observers for IQFinv, 5 observers for ROC).

We defined the optimal dose as the point at which IQFinv or AUC suddenly changed. This point was taken as the intersection point of the approximate straight line of the group of points having no significant difference ($P>0.05$) and the group of points having a significantly different slope ($P<0.05$) by T test for IQFinv or AUC values of the reference dose or 0.75 times the reference dose.

2.3.3. Ethical consideration

Participants' rights as the observers were clearly written and explained, assuring them that the data would only be used for research purposes and that their confidentiality would be protected. Participants were informed that they were free to refuse or withdraw at any time. The research was approved in writing by the observers.

3. Results

Digital characteristic curves are shown in Figure 2. The relationship between the logarithmic values of the doses

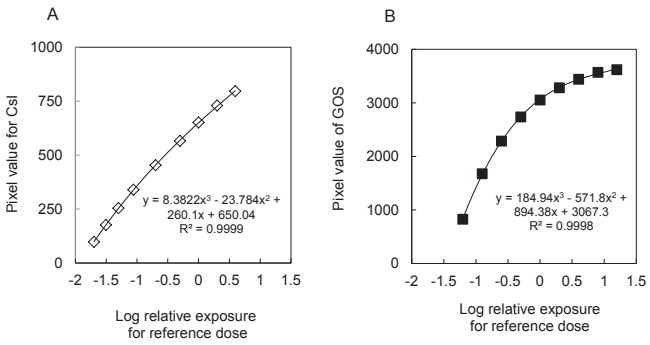

Fig. 2. Digital characteristic curves for the CsI and Gd_2O_2S:Tb (GOS) types of irradiation side sampling flat-panel detectors (ISS-FPDs): A, CsI type; B, GOS type.

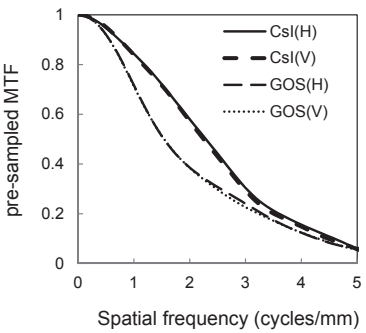

Fig. 3. Comparison of the pre-sampled modulation transfer function (MTF) for the CsI and Gd_2O_2S:Tb (GOS) types of irradiation side sampling flat-panel detectors (ISS-FPDs) in the vertical (V) and horizontal (H) directions.

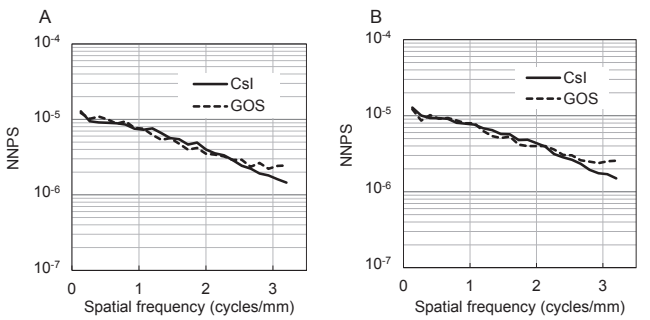

Fig. 4. Normalized noise power spectrum (NNPS) for the CsI and Gd_2O_2S:Tb (GOS) types of irradiation side sampling flat-panel detectors (ISS-FPDs) in the vertical (A) and horizontal (B) directions under the reference dose exposure condition.

and the pixel values was a cubic function for both CsI and GOS.

Pre-sampled MTFs are shown in Figure 3. These confirm that CsI has higher resolution. The pre-sampled MTFs of the CsI were higher than those of the GOS by approximately 18% in a spatial frequency of 1 cycle/mm, and by approximately 49% in 2 cycles/mm both in the vertical and horizontal directions.

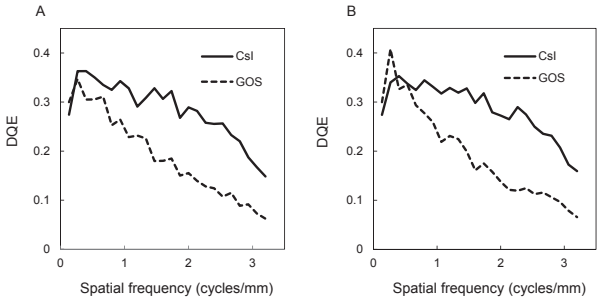

Fig. 5. Detective quantum efficiency (DQE) for the CsI and Gd_2O_2S:Tb (GOS) types of irradiation side sampling flat-panel detectors (ISS-FPDs) in the vertical (A) and horizontal (B) directions under the reference dose exposure condition.

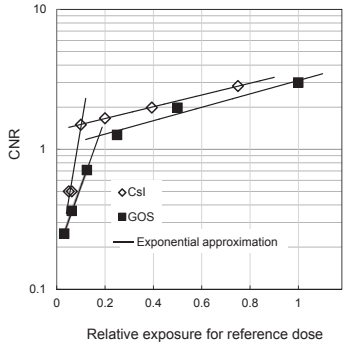

Fig. 6. Contrast-to-noise ratio (CNR) for the CsI and Gd_2O_2S:Tb (GOS) types of irradiation side sampling flat-panel detectors (ISS-FPDs) under various exposure conditions: The relative exposures at the intersection of the approximated curves are 0.10 (CsI) and 0.18 (GOS), respectively.

Table 2. Detective quantum efficiencies (DQEs) ratio of Gd_2O_2S:Tb (GOS) to CsI types of irradiation side sampling flat-panel detector (ISS-FPD)

Spatial frequency	Vertical direction	Horizontal direction
1 cycles/mm	0.74	0.74
2 cycles/mm	0.54	0.51
3 cycles/mm	0.46	0.46
Average	0.58	0.57

NNPSs are shown in Figure 4A and B. There was a very small difference in NNPSs between the CsI and GOS in either the vertical or horizontal directions.

DQEs are shown in Figure 5A and B. We observed that the DQEs of the CsI were higher than those of the GOS in both the vertical and horizontal directions. For the vertical direction, at 1, 2, and 3 cycles/mm, DQE values of the CsI were 0.34, 0.29, and 0.18, respectively, and those of the GOS were 0.25, 0.16, and 0.08, respectively. For the horizontal direction, those of the CsI were 0.32, 0.27, and 0.19, respectively, and those of the GOS were 0.24, 0.14, and 0.09, respectively. DQE ratios of the GOS to the CsI in each frequency are shown in Table 2. The GOS showed

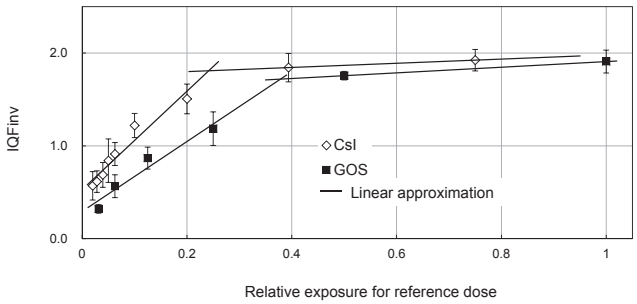

Fig. 7. Inverse image quality figure (IQFinv) for the CsI and Gd_2O_2S:Tb (GOS) types of irradiation side sampling flat-panel detectors (ISS-FPDs) under various exposure conditions: The relative exposures at the intersection of the approximated straight lines are 0.24 (CsI) and 0.38 (GOS), respectively. Markers correspond to the mean ± SD of 7 observers.

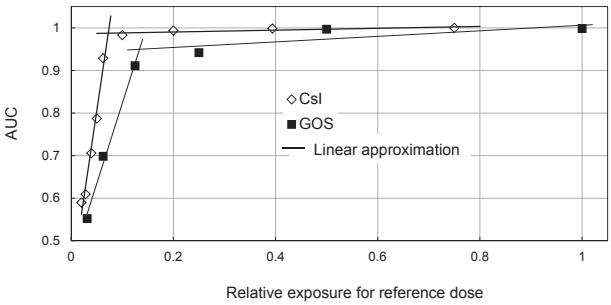

Fig. 8. Area under the curve (AUC) of the receiver operating characteristics (ROC) curve for the CsI and Gd_2O_2S:Tb (GOS) types of irradiation side sampling flat-panel detectors (ISS-FPDs) under various exposure conditions: The relative exposures at the intersection of the approximated straight lines are 0.07 (CsI) and 0.13 (GOS), respectively. Markers correspond to the mean ROC from 5 observers.

Table 3. Optimal dose ratio of CsI to Gd_2O_2S:Tb (GOS) types of irradiation side sampling flat-panel detector (ISS-FPD)

	Ratio DQE (GOS/CsI)		Optimal dose ratio (CsI/GOS)
	Vertical direction	Horizontal direction	
DQE	0.58	0.57	0.58

	Relative exposure for reference dose		Optimal dose ratio (CsI/GOS)
	Change-point of CsI	Change-point of GOS	
CNR	0.10	0.18	0.56
IQFinv	0.24	0.38	0.63
AUC	0.07	0.13	0.54

an average value of approximately 58% of that from CsI.

CNRs are shown in Figure 6. We observed that the CNRs of the CsI were higher than those of the GOS for all relative exposure doses. If we assume that the optimal dose is the point at which the CNR suddenly changes, we can derive two approximate curves. The relative exposures for the reference dose of the intersections of the CsI and the GOS were 0.10 and 0.18, respectively.

Results of the visual evaluation are shown in Figures 7 and 8. IQFinv values of the CsI were higher than those of the GOS (Fig. 7). If we assume that the optimal dose is the point at which the IQFinv suddenly changes, we can derive two approximate straight lines. The relative exposures for the reference dose of the intersections of the CsI and the GOS were 0.24 and 0.38, respectively. Furthermore, the AUCs of the ROC curve of the CsI were higher in comparison with those of the GOS (Fig. 8). If we assume that the optimal dose is the point at which the AUC suddenly changes, we can derive two approximate straight lines. The relative exposures for the reference dose of the intersections of the CsI and the GOS were 0.07 and 0.13, respectively.

Table 3 shows the optimal dose ratio of CsI to GOS. The optimal dose ratio of DQE shows the average of the DQE ratios in the vertical and horizontal directions. The optimal dose of CsI was 54-63% that of GOS for all of DQE, CNR, IQFinv and AUC.

4. Discussion

We measured quantitative and visual image quality metrics from ISS-FPDs with different scintillators. The resolution of CsI, as per the MTF, was better than that of GOS. Noise characteristics, measured as per the NNPS, showed comparable performance for both CsI and GOS. The DQE value for GOS was approximately 58% that of CsI. The reciprocal of the DQE ratio is considered to be the dose ratio required to obtain the same image quality[3, 23]. That is, CsI may be able to capture images at a lower dose of 58% compared to GOS whilst obtaining equivalent image quality. In other words, there is a possibility that CsI can reduce by 42% the exposure dose of GOS. GOS DQE has also been reported as 58% (at 1 cycle/mm in RQA5) of CsI in another study[3], which is the same as the result presented here. It should be noted, however, that both the manufacturer of the CsI scintillator and the X-ray quality used in that and the present study were different. By evaluating CNR, the optimal dose of CsI was 56% that of GOS, which is similar to the DQE results. Therefore, in terms of image quality, there is a possibility that CsI can reduce by 42-44% the exposure dose of GOS.

The optimal dose in the visual evaluation is the minimum dose that can be used for diagnosis in clinical images[3]. In phantom images, this is set as the minimum dose of the flat part of the IQF or the AUC[19]. Regarding the image quality index, IQFinv increases with increasing dose because graininess improves with increasing dose. However, this change in IQFinv differs between the low dose range and the high dose range. In the low dose range, quantum noise is dominant, so the change in IQFinv is large. However, in the high dose range, system noise is dominant, so the change in IQFinv is small. Mochizuki *et al*. set the threshold at the intersection of two straight lines depicting the quantum noise region and the system noise region as a value that did not contribute to improvement in image quality even when the dose was increased[19]. Regarding the AUC, it plateaued at high doses, and the boundary between the area with large change and the plateau was assumed to be the optimal dose[19]. Based on these considerations, we chose the intersection of two approximate straight lines depicting the quantum noise region and the system noise region as the optimal dose in the present study. As a result, the optimal doses of CsI by visual assessment of IQFinv and AUC were 63% and 54% those of GOS. Therefore, in terms of the visual evaluation, there is a possibility that CsI can reduce by 37-46% the exposure dose of GOS. Use of IQFinv and AUC in an approximate method for optimal dose estimation demonstrated that the estimates of both were close, so this method was considered to be appropriate and effective for dose estimation. Furthermore, these results were similar to the image quality evaluation results using DQE and CNR.

The DRL reference material provides a dose comparison of CR and FPD, which has been shown to be 30-40% less in FPD than in CR[9]. Due to the differences between CsI and GOS, and between ISS and PSS, exposure doses are different in FPD systems as well. Therefore, determining the optimal dose of the FPD to be used is needed for reducing the exposure dose. In this study, we clarified the difference in the optimal dose of CsI and GOS ISS-FPD systems. The quality of the X-rays used in this experiment was RQA7, but the quality of radiation varies at different facilities, which has to be taken into account for dose reduction.

5. Conclusion

In order to investigate reducing exposure dose while maintaining image quality, we measured image quality and performed a visual evaluation on the images obtained from different scintillators of ISS-FPDs. The optimal dose of the CsI type ISS-FPD system produced 54% to 63% better quality images than those from the GOS type ISS-FPD system. Therefore, the CsI type ISS-FPD system could possibly reduce by approximately 40% (37-46%) the exposure dose of the GOS ISS-FPD system.

Acknowledgements

I am deeply grateful to the students of The School of Health Sciences, Medical Department at Hirosaki University, Mr. Morito Osanai, Mr. Masaya Kudo, Mr. Shunnosuke Goto and Mr. Nobuhiro Komiya, who cooperated with me in this study.

Conflict of Interest Disclosure

The authors declare that they have no conflict of interest.

References

1. Yamada S. Development of a direct-conversion-type flat-panel detector for radiography and fluoroscopy. Med Imaging Technol. 1999;17(2):1106.
2. Yamazaki T, Morishita M, Kaifu N and Endo Y. Development of flat panel digital radiography system. Med Imaging Technol. 1999;17(2):117–22.
3. Kishimoto K, Ariga E, Ishigaki R, Imai M, Kawamoto K, Kobayashi K, *et al*. Study of appropriate dosing in consideration of image quality and patient dose on the digital radiography. Jpn J Radiol Technol. 2011;67:1381–97. Japanese.
4. Yamazaki T. Technology in indirect flat-panel detector. J Soc Photogr Sci Technol Jpn. 2007;70 (Suppl) :24–5. Japanese.
5. Sato K, Nariyuki F, Kuwabara T, Fukui S, Okada Y, Nabeya T, *et al*. Development of "CALNEO", an indirect-conversion digital radiography system with high-conversion efficiency. Fujifilm Res Dev. 2010;55:10–3. Japanese.
6. Kitada M, Bettouyashiki A, Shimizukawa S, Tajima T and Ogura R. Development of next-generation ultra-lightweight cassette DR "CALNEO smart". Fujifilm Res Dev. 2015;60:6–9. Japanese.
7. ICRP. The 2007 Recommendations of the International Commission on Radiological Protection, ICRP Publication 103. Ann. ICRP 37. 2–4, 2007.
8. ICRP. Radiological Protection in Medicine. International Commission on Radiological Protection, ICRP Publication 105. Ann. ICRP 37. 6, 2007.
9. Japan network for research and information on medical exposure. Diagnostic reference levels based on latest surveys in Japan—Japan DRLs 2015—. J- RIME, Japan, 2015. Japanese.
10. Tanaka N, Yano Y, Yabuuchi H, Akasaka T, Sasaki M, Ohki M, *et al*. Basic imaging properties of an indirect flat-panel detector system employing irradiation side sampling (ISS) technology for chest radiography: comparison with a computed radiographic system. Radiol Phys Technol. 2013;6:162–9.
11. Kudo K, Osanai M, Hirota J, Abe T, Matsuoka M, Naraki S, *et al*. Comparison between irradiation side sampling flat-panel detector system and computed radiography system for reduction of radiation exposure. Radiat Environ Med. 2015;4:45–52.
12. Fujita T and Anno H. X-ray flat panel detectors and X-ray tubes contributing to development of X-ray diagnostic systems. Toshiba Review 2011;66:24–8. Japanese.
13. IEC 62220-1 Ed. 1.0 Medical electrical equipment—characteristics of digital X-ray imaging devices—part 1: determination of the detective quantum efficiency. The International Electrotechnical

Commission. 2003.

14. IEC 61267 Ed. 1.0 Medical diagnostic X-ray equipment—radiation conditions for use in the determination of characteristics. The International Electrotechnical Commission. 1994.
15. Yokoi T, Takata T and Ichikawa K. Investigation of image quality identification utilizing physical image quality measurement in direct- and indirect-type of flat panel detectors and computed. Jpn J Radiol Technol. 2011;67:1415–24. Japanese.
16. Nagashima C, Uchiyama N, Moriyama N, Nagata Mio, Kobayashi H, Sankoda K, *et al*. Evaluation of the 1shot phantom dedicated to the mammography system using FCR. Jpn J Radiol Technol. 2009;65:921–30. Japanese.
17. Kawamura T, Naito S, Okano K and Yamada M. Improvement in image quality and workflow of X-ray examinations using a new image processing method, "Virtual Grid Technology". Fujifilm Res Dev 2015;60:21–7. Japanese.
18. Ito R, Takagi T, Yoshida K and Ishisaka A. Development of the intelligent grid scattered X-ray correction processing system for digital radiography. Konica Minolta Technology Report. 2016;13:52–6. Japanese.
19. Mochizuki Y, Abe S and Yamaguchi K. Estimation of appropriate dose for computed radiography by the threshold value of the image quality figure. Jpn J Radiol Technol. 2009;65:430–7. Japanese.
20. Ogawa W, Nakaya G and Karasawa H. Fitting of ROC curves for continuous data by using correction of the mean and standard deviation. Jpn J Radiol Technol. 2004;60:111–7. Japanese.
21. Ichikawa K and Ishida T. Image quality measurement of digital radiography. pp.109–224. Ohm-Sha, Tokyo. 2011. Japanese.
22. Kawaharada M, Ishida T, Okura Y and Kawashita I. Relationship between image quality and signal detectability in CR and FPD Systems. Jpn J Radiol Technol. 2010;66:1449–56. Japanese.
23. ICRP. Managing patient dose in digital radiology. International Commission on Radiological Protection, ICRP Publication 93. Ann. ICRP 34.1, 2004.